AN INTEGRATED ENVIRONMENT FOR HELICOPTER AEROSERVOELASTIC ANALYSIS: THE GROUND RESONANCE CASE

Pierangelo Masarati, Vincenzo Muscarello, Giuseppe Quaranta

Dipartimento di Ingegneria Aerospaziale, Politecnico di Milano
{masarati,muscarello,quaranta}@aero.polimi.it

Alessandro Locatelli, Daniele Mangone, Luca Riviello, Helicopter System Design
Luca Viganò, Automatic Flight Control Systems

AgustaWestland
{alessandro.locatelli,daniele.mangone,luca.riviello,luca.vigano}@agustawestland.com

Abstract

The introduction of Flight Control System in modern rotorcraft calls for an improvement of the classical aeromechanics analysis methods used to investigate the dynamic stability of this kind of machines. It is important to consider from the preliminary design phase the analysis of Structural Coupling problems, i.e. those problems related to the interaction of the Flight Control System with high frequency structural dynamics. This paper presents an effective approach to develop multidisciplinary models that can tackle this peculiar type of problems. To better explain its potential, the proposed approach is applied to the investigation of structural coupling problems that may arise in the stability analysis of ground resonance.

1 INTRODUCTION

Flight Control Systems (FCS) are an essential part of modern rotorcraft. The expected enhancements in terms of handling qualities and reduction of pilot workload, with the promise of greater safety, are increasing the number of rotorcraft designs equipped with sophisticated FCS [1]. The aircraft FCS sets up a feedback loop between the measures coming from Inertial Sensors (IS) and the controls. Even though the FCS is usually designed to control essentially the rigid body motion, the IS are fitted into the deformable airframe, and thus they pick up structural vibrations as well, unless appropriate filtering is used. This spill-over may cause problems when the FCS responds to aeroelastic excitation. Consequently, the introduction of the FCS requires its inclusion in the aircraft design phase to verify that it does not compromise the overall aeroelastic stability and vibratory level. The investigation of the possible coupling between the dynamic response of the airframe and the FCS is currently denominated Structural Coupling (SC), and plays a very important role in the qualification of aircraft with digital control. SC procedures are well assessed in the fixed wing community [2] while less literature is available on rotary wing aircraft.

It may be important to have a simple, modular and effective tool that allows to perform aeroservoelastic analysis from the preliminary rotorcraft design phase, considering different levels of detail for both the FCS and the actuators, to anticipate as many SC problems as possible. They must allow to investigate the interaction between different subsystems like deformable mechanical components, servo-hydraulic elements, unsteady aerodynamic loads, pilot models, control systems and so on. Several numerical approaches with different level of sophistication have been implemented in the past to study rotorcraft aeromechanics. Noteworthy examples are presented in [3–7]. Perhaps a less general, more “control oriented” approach is represented by ASAP [8], developed to investigate SC problems for tiltrotor fly-by-wire architectures.

Instead of developing yet an entirely new rotorcraft aeroservoelastic simulation software, a tool called MASST (Modern Aeroservoelastic State-Space Tools) has been created on top of a general-purpose mathematical environment, exploiting Graphical User Interfaces (GUI) to make it easily usable. The tool can perform massive analyses of relatively simple, yet complete modular models of complex linear(-ized) aeroservoelastic

systems [9]. Each separate component consists of sub-models collected from well-known, reliable and state-of-art sources blended together, rather than deriving them from first principles equations. Since a time domain formulation in state-space is at the core of the modern control theory, the equations of motion of the system are cast as first order time differential equations. Once this is accomplished, it is no longer necessary to use the specialized formulations generally adopted in aeroelastic analysis; general state-space approaches can be rather used to analyze aeroservoelastic systems.

As a paradigmatic SC case for helicopters we propose here to analyze the possible interaction of FCS with the classical Ground Resonance (GR) problem [10]. Several studies have been performed on the possibility to use the FCS as a means to cancel GR problems [11, 12]. This work rather focuses on the effects of a FCS designed for flight-mechanics purposes on GR stability.

Section 2 of the paper presents the basic elements of the numerical environment MASST. Section 3 describes the multidisciplinary model built using MASST for GR analysis, and presents the main results obtained on the effect of FCS on ground resonance. In this case both linear stability analysis and SC analysis through gain and phase margins are presented.

2 MULTIDISCIPLINARY MODEL WITH MASST

MASST has been designed to be modular and to incorporate heterogeneous sub-components from different sources to model:

1. airframe structural dynamics, including unsteady aerodynamics;
2. rotor aeroelasticity;
3. drive train;
4. servo-actuation systems;
5. sensors and filters;
6. Flight Control Systems;
7. pilot biomechanics.

An arbitrary number of blocks for each component type can be added to the main model, to allow to build aircraft models of arbitrary architecture. Items 1–3 provide the core of basic aeroelastic analysis capabilities. Items 1–4 provide aeroservoelastic analysis capabilities. Items 1–7 provide closed loop aeroservoelastic capabilities.

Each component is modeled in its most natural and appropriate modeling environment and then cast into first order state-space formulation. Substructures are then connected using Craig-Bampton's Component Mode Synthesis (CMS) approach [13].

Airframe Structural Dynamics

The non-rotating aeroelastic subsystems can be logically split in structural and aerodynamic models, since the structural model does not depend on the flight condition, while the aerodynamic model can be parametrized on flow parameters, e.g. Mach number and dynamic pressure. The airframe structural models are represented by a Reduced Order Model (ROM) obtained using the classical Ritz decomposition for the displacement field $\mathbf{u}$

$$\mathbf{u}(\mathbf{x},t) = \mathbf{U}(\mathbf{x})\mathbf{q}(t), \tag{1}$$

based on a compact set of selected generalized coordinates $\mathbf{q}$. Usually the model is obtained by reducing a detailed Finite Element Model (FEM) using displacement shapes $\mathbf{U}$ chosen among the normal vibration modes of the structure, complemented with additional *constraint modes*, namely static shapes specifically designed to represent local effects, or control modes that represent the motion of control surfaces. The structural dynamics is thus represented by

$$\mathbf{M_{qq}}\ddot{\mathbf{q}} + \mathbf{C_{qq}}\dot{\mathbf{q}} + \mathbf{K_{qq}}\mathbf{q} = \mathbf{f}, \tag{2}$$

where matrices $(\cdot)_{\mathbf{qq}}$ are symmetric, but in general fully populated since no orthogonality is required for the shapes $\mathbf{U}$. The airframe structure can be composed of an arbitrary number of substructures connected using the CMS. The aim is twofold: a) to parametrize the model in terms of the relative orientation of parts, as required for example by tiltrotor nacelles; b) to be able to temporarily add/remove sub-components like pylons or appendages to/from a model. Unsteady aerodynamic forces can be added to the airframe according to the approach described in [9].

Rotor Aeroelasticity

Linearized rotor modeling is more challenging than that of the airframe. In fact, in this case even the isolated component cannot be considered linear, since it presents a significant dependence on the parameters $\mathbf{p}$, for example the trim conditions [14]. For this reason the aeroelastic models of the rotors have been considered as monolithic

blocks composed by the joined structural and aerodynamic equations in the form

$$\mathbf{A}_2(\mathbf{p})\ddot{\mathbf{q}}_r + \mathbf{A}_1(\mathbf{p})\dot{\mathbf{q}}_r + \mathbf{A}_0(\mathbf{p})\mathbf{q}_r = \mathbf{B}_g(\mathbf{p})\mathbf{v}_g + \mathbf{f}_c(\mathbf{p}), \tag{3}$$

where $\mathbf{q}_r$ are global rotor degrees of freedom chosen using the Ritz decomposition of Eq. (1) as discussed for the airframe, matrices $\mathbf{A}_0$, $\mathbf{A}_1$, $\mathbf{A}_2$, $\mathbf{B}_g$ are Linear Time Invariant (LTI), computed using coefficient averaging to eliminate any periodicity whenever the rotor is not in axial flow conditions [14], and vector $\mathbf{f}_c$ represents the forces applied by the servo-actuators on the rotor to control the blade collective and cyclic pitch angles. Eq. (3) represents a quasi-steady, LTI approximation of the rotor dynamics, that depends on specific operating (rpm, Mach number, dynamic pressure) and trim (shaft angle, reference control angles) conditions. The state $\mathbf{q}_r$ contains an arbitrary number of rotor elastic modes, expressed in the non-rotating reference frame using the multiblade transform [14], plus six rigid rotor hub motion modes used as *constraint modes* to connect the rotor to the corresponding airframe model with the CMS approach [13]. Each linearized rotor model is related to a set of parameters $\mathbf{p}$ used to characterize it. These parameters are composed by a set that is related to the rotor trim condition, plus possible additional parameters defined by the user. These may include for example elements like a characteristic stiffness or damping value (like those of the lead lag damper), a characteristic rotor geometrical parameter like the δ_3 angle and so on. The linearized model can be generated using comprehensive rotorcraft solvers, as soon as it is provided in the rather general form of Eq. (3); CAMRAD/JA [3] has been used in this work.

The strong dependence of the matrices in Eq. (3) on the set of parameters $\mathbf{p}$ ideally requires to assemble a specific model for each flight condition considered during the aeroservoelastic analysis. This approach has not been considered suitable for the purpose of implementing a fast analysis tool. On the contrary, a robust interpolation method is used to estimate rotor models for any intermediate parameter point from a discrete database of linearized models pre-computed for several trim conditions. Each point of the database is characterized by a parameter vector $\mathbf{p}_i$ of size m, the number of parameters, so the entire database composed by N points can be defined as $\mathcal{P} = \{\mathbf{p} \in \Omega \subset \mathbb{R}^m, \mathbf{p} = \mathbf{p}_i \qquad i = 1, \ldots, N\}$, where Ω is a compact subspace of the parameter space. The models can be interpolated according to the algorithms:

1. **Nearest neighbor:** given a query point $\mathbf{p}_q$ in the parameter space at which the data needs to be approximated, MASST looks for the nearest point in the parameter space, and approximates the query model with the nearest model.
2. **Linear interpolation through m-dimensional tessellation:** the linear interpolation is obtained by generating a m-dimensional tessellation of the space of the parameters using the Delaunay approach. The space of the parameters is decomposed in S, m-dimensional, simplices T with vertexes in the points available in the database. Thus, given a point $\mathbf{p}_q$, the algorithm proceeds by identifying the enclosing simplex of the specified point, and then applies the linear interpolation using the vertexes of the selected simplex as known values.
3. **Moving Least Squares:** to achieve significant freedom in the choice of the reference conditions used to populate the database, a technique that allows interpolation starting from a set of point-wise scattered data is used. The Moving Least Square (MLS) approach meets this requirement. The mathematical details of the techniques can be found in [15]. The result obtained is a local polynomial approximation up to the order chosen by the user, with a global smoothness of the resulting interpolated data that can be defined by the choice of the weight function.

Usually an initial compact database composed of few computed models can be sufficient to frame the critical zones on the parameter space. Subsequently, additional points can be included in those zones to gain additional precision for the simulation results. The rotor model can be re-computed at selected flight conditions, to verify the quality of the interpolation.

Servo-actuators

Servo-actuators are modeled as equivalent transfer-functions. The transfer function of a servo-actuator usually describes the motion of a generic control surface, β, as a function of the requested motion, β_c, and of the generalized reaction force applied by the dynamics of the control surface itself, m_c, (see [16, 17]), namely

$$\beta = H_\beta(s)\,\beta_c + H_M(s)\,m_c. \tag{4}$$

In general, both the servo-valve and compliance dynamics are fully represented by transfer functions $H_\beta(s)$ and $H_M(s)$, respectively. The corresponding expression of the generalized force m_c applied to the controlled surface is

$$m_c = \frac{1}{H_M(s)}\left(\beta - H_\beta(s)\,\beta_c\right), \tag{5}$$

provided the dynamic compliance $H_M(s)$ is not strictly proper. Otherwise, a dynamic residualization up to second order can be applied without breaking the causality of the overall system, since the structural dynamics of the connected element is second-order differential in time, and thus β is available with its derivatives $\dot{\beta}$ and $\ddot{\beta}$. The generalized force becomes

$$m_c = m_M s^2\beta + c_M s\beta + \frac{1}{\hat{H}_M(s)}\left(\beta - H_\beta(s)\,\beta_c\right), \tag{6}$$

where $\hat{H}_M(s)$ is a proper transfer function. The resulting transfer functions need to be transformed in the time domain to obtain a state-space model of the actuator.

The actual motion of the control surface, β, is then expressed as a function of the structural states, $\beta = \mathbf{U}_\beta\mathbf{q}$, and the transfer function is added to the problem using the Principle of Virtual Work (PVW), namely

$$\delta\mathcal{L}_M = \delta\beta^T m_c = \delta\mathbf{q}^T\mathbf{U}_\beta^T\frac{1}{H_M(s)}\left(\mathbf{U}_\beta\mathbf{q} - H_\beta(s)\,\beta_c\right). \tag{7}$$

Servo-actuators of airframe control surfaces like ailerons, flaps, elevators and rudders can be modeled with this approach. Rotor servo-actuators can be introduced as well by restoring the load path between the blade pitch motion and the airframe structural dynamics. For simplicity, the formulation is presented only for the collective pitch motion. With the multiblade transformation the generalized theory can be formulated for the complete blade pitch motion, also considering the cyclic contributions.

The blade pitch dynamics equation is

$$\begin{aligned}\delta\mathcal{L}_M = {} & \delta\vartheta^T I_f\ddot{\vartheta} + \delta\vartheta^T I_f\Omega^2\vartheta \\ & + \delta(\vartheta-\vartheta_0)^T K_{T0}(\vartheta-\vartheta_0) + \delta x^T f_c,\end{aligned} \tag{8}$$

where I_f represents the moment of inertia about the feathering axis of the blade, Ω is the rotor rpm, K_{T0} is the collective stiffness of the control chain, and f_c is the reaction force due to the servo-actuator; ϑ is the blade pitch angle, while ϑ_0 is the pitch angle commanded by the servo-actuator and x represents the servo actuator extension.

The contributions to the blade pitch equation are: (1) the feathering inertia $I_f\ddot{\vartheta}$, (2) the propeller moment $I_f\Omega^2\vartheta$, (3) the restoring moment $K_{T0}(\vartheta-\vartheta_0)$ due to the flexibility of the control chain, and (4) the servo-actuator reaction force f_c.

The extension of the servo-actuator is a function of the structural states, $x = \mathbf{U}_x\mathbf{q}$, while the pitch angle ϑ_0 is related to the servo-actuator through the kinematic gear ratio η, so that $\vartheta_0 = \eta x = \eta\mathbf{U}_x\mathbf{q}$.

As in Eq. (5), the reaction force applied by the servo actuator is

$$f_c = \frac{1}{H_f(s)}\left(x - H_x(s)\,x_c\right), \tag{9}$$

considering the servo-valve dynamics $H_x(s)$ and the dynamic compliance $H_f(s)$. The displacement x_c requested to the servo-actuator is a function of the blade pitch request ϑ_c generated by the pilot/FCS by means of the inverse of the kinematic gear ratio, $x_c = \vartheta_c/\eta$. Equation (8) becomes

$$\begin{aligned}\delta\mathcal{L}_M = {} & \delta\vartheta^T I_f\ddot{\vartheta} + \delta\vartheta^T I_f\Omega^2\vartheta \\ & + \delta(\vartheta-\eta\mathbf{U}_x\mathbf{q})^T K_{T0}(\vartheta-\eta\mathbf{U}_x\mathbf{q}) \\ & + \delta\mathbf{q}^T\mathbf{U}_x^T\frac{1}{H_f(s)}\left(\mathbf{U}_x\mathbf{q} - H_x(s)\,\frac{1}{\eta}\vartheta_c\right).\end{aligned} \tag{10}$$

The cross-coupling terms between the blade pitch motion, the airframe structural dynamics and the servo-actuator dynamics are related to the control system load path, rebuilt along the different sub-components. Moreover, the pilot/FCS input allows to introduce the pilot/FCS feedback to perform closed loop aeroservoelastic analyses.

Generally, pitch/bending and pitch/gimbal kinematic couplings must be taken into account when restoring the control chain moment $m_{\text{con}} = K_{T0}(\vartheta-\vartheta_0)$. In this case

$$\vartheta_0 = \eta\mathbf{U}_x\mathbf{q} - \sum_i K_{p_i}q_{ei} - K_{p_G}\beta_G, \tag{11}$$

where the term $-K_{p_i}q_{ei}$ is the kinematic pitch/bending coupling due to control system and blade root geometry, and q_{ei} is the i^{th} bending degree of freedom of the rotor. Similarly, K_{p_G} is the pitch/flap coupling for the gimbal or teetering motion. The effect of local nonlinearities of the actuator, like freeplay, saturation and deadband, can be taken into account.

Sensors and Filters Dynamics

Sensors range from the direct extraction of the motion of a physical point as a function of the

states of the system to the inclusion in the model of the dynamics of the sensor itself. In the latter case, the transfer function of the sensor is added after transforming it into the time domain in state-space form.

Flight Control System

The Flight Control System represents a key element of modern rotorcraft. For the purpose of MASST, under the generic name of "Flight Control System" are grouped together all FCS components that have a significant impact on rotorcraft aeroservoelasticity and have not been already included in the Actuation and Sensors subsystems.

3 GROUND RESONANCE WITH FCS

In general, GR is a dynamic instability that involves the coupling of the cyclic lag motion of the blades with the in-plane motion of the rotor hub. This instability is characterized by a resonance of the frequency of the rotor lag motion (specifically the regressive cyclic lag mode) and a natural frequency of the structure supporting the rotor. A resonance is possible when the rotating lag frequency ν_ζ is below 1/rev, as for articulated and soft-inplane hingeless rotors. With articulated rotors, the critical mode is usually an oscillation of the helicopter on the landing gear when in contact with the ground, hence the name Ground Resonance. The foundations of the research on Ground Resonance have been laid by the work of Coleman and Feingold [10]. Sometimes the phenomenon can occur in flight as well, due to the coupling of the lead-lag cyclic modes with the low frequency airframe modes related to flight dynamics; in this case it is called Air Resonance (AR). Ground resonance is potentially destructive; avoiding this instability is an important consideration in helicopter design. Generally, resonances above 120% of the nominal operating speed or below 40% of it are acceptable. For a fairly broad range about the nominal rotor speed it is therefore necessary to either avoid resonances or provide sufficient damping in the system to prevent any instability. Basic models of this instability consider essentially the interaction between the rotor lead-lag motion and the low frequency fuselage modes that displace the center of the rotor; aerodynamic forces are often neglected [10, 18]. However, when the FCS is included in the loop, additional paths may have an influence on the GR, as stated in [19]:

1. the lead-lag damping is influenced by the in-plane aerodynamics and Coriolis forces generated by the flapping motion that is controlled by the blade pitch;

2. the rotor moments generated by the flap motion due to pitch input may modify the oscillations of the fuselage.

As a consequence, the modeling of rotor flap and pitch modes becomes important for the analysis of SC, because through these modes the FCS is able to pump energy into the GR instability mechanism. As a consequence aerodynamic forces should not be neglected.

The identification of SC effects often leads to insertion of filters on sensors. They represent a widely used tool that allows to avoid or fix spill-over problems caused by the coupling of the FCS with higher frequency structural dynamics modes [20]. The possibility to quickly filter out undesired signals directly in the aeroelastic model, minimizing the impact on the FCS performances, represents an extremely useful feature. Ideally, it is also possible to avoid SC effects that lead to ground resonance by switching to a different control scheme in Weight-on-Wheels conditions. However, this approach has often shown a tendency to develop Rotorcraft-Pilot Coupling (RPC) [21] occurrences, because the mode switch of FCS may cause a pilot mental model mismatch to develop [1, 22, 23].

Model description

For the GR analysis the characteristic of a medium size helicopter are considered. In order to test the possibility of using MASST to predict ground resonance with FCS in the loop, the helicopter model has been augmented with a realistic control system. The bandwidth of the FCS, without any input and/or output filtering, is high enough to potentially interact with the elastic modes of the airframe. Aeroservoelastic and aeromechanical analyses have been performed to evaluate the SC behavior. A block scheme of the complete model is shown in Figure 1.

The airframe model is composed by 5 vibration modes of the helicopter on ground. In this case the model is very simple, composed by modal, mass,damping and stiffness values plus the displacement at few noteworthy points like the center of the main and tail rotor hubs, the sensor positions and so on. The main rotor models are derived using a CAMRAD/JA model, and are parametrized at different operating speeds (rpm) and thrust values. The main rotor lead-lag dampers are not part

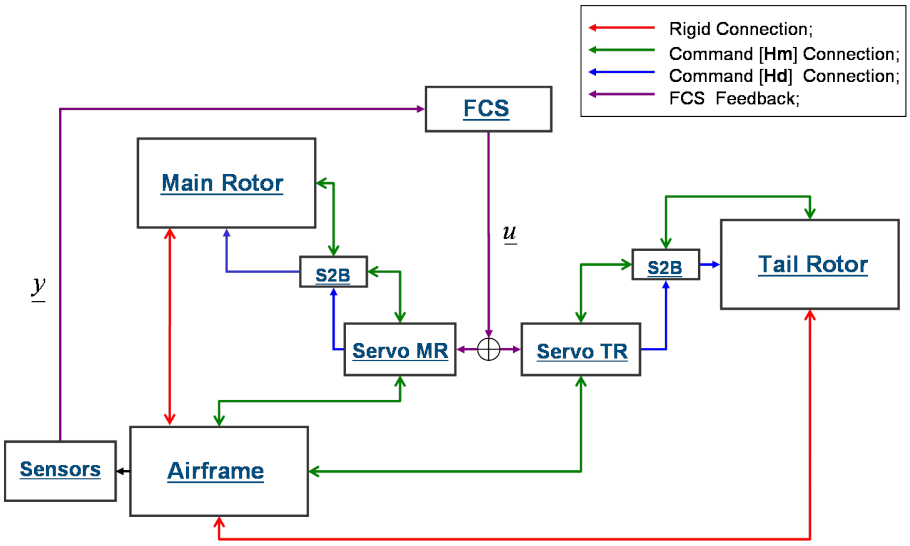

Figure 1: Block diagram of the helicopter aeroservoelastic model.

of the main rotor model, but are rather considered as external additional elements, in order to allow a thorough investigation of the GR behavior with respect to their characteristics without the necessity to generate too large a main rotor model database. The viscoelastic lead-lag restoring torque Q_ζ generated by the dampers can be modeled as a function of the lead-lag rotation ζ and angular velocity $\dot{\zeta}$ at the lag hinge by introducing the simple relation

$$Q_\zeta = -K_\zeta \zeta - C_\zeta \dot{\zeta}. \tag{12}$$

De facto this element introduces a feedback path between the sensors of rotation and angular velocity measured at the lead-lag hinges and the restoring torques Q_ζ acting on the same hinges, that can be easily modeled in MASST as a controller. The Tail Rotor (TR) aeroelastic models are also derived in CAMRAD/JA, and are parameterized at different operating speeds (rpm), with TR collective in mid position. The degrees of freedom of the MR and TR models are composed by the first two blade bending modes (the first in lag and flap directions), and the first torsional mode. Typical linear servo transfer functions, including both terms of Eq. (5), are defined for the three actuators of the main rotor swashplate, and for the single actuator of the tail rotor. A gear ratio matrix, called "Servo To Blade", is used to convert the actuator displacements into collective and cyclic commands. Finally, the model includes three sensors for the angular rates p, q, r and the FCS that connects the angular rates of the airframe with the main and tail rotor actuators.

4 Linear Stability Analysis Results

Figure 2 shows the behavior of the helicopter eigenvalues for different values of angular velocity without lead lag dampers. All the eigenvalues have been divided by the nominal rotational speed, so the data shown are non-dimensional. The typical instability "bubbles" appear; one, centered around 40% rpm, is due to the interaction of the lead-lag cyclic regressive mode with the lateral oscillation mode of the airframe; a second one, centered at 120% rpm, is due to the interaction of the lead-lag cyclic regressive mode with the roll oscillation mode of the airframe. After adding an appropriate lead-lag damper, the correct behavior is recovered as expected and no instability appears, as shown in Figure 3. When the FCS is added an instability appears close to 110% rpm as shown by the eigenvalue diagram of Figure 4. In this case the airframe roll mode becomes unstable. To understand the effect of the FCS on the system it is useful to analyze the behavior of the damping of the helicopter roots without activating the lead-lag rotor modes. Figure 5 shows how the damping of the roll mode with the FCS on reduces when the rpm increases, since the real part of the eigenvalue becomes less negative, while with the FCS off the damping of the same mode increases continuously. The FCS senses the roll motion of the airframe and responds with an input of blade pitch variation; this input causes a flapping motion of the blades that reduces the damping of the roll mode. In this case, the path related to the rotor moment transmitted to the airframe roll motion causes this

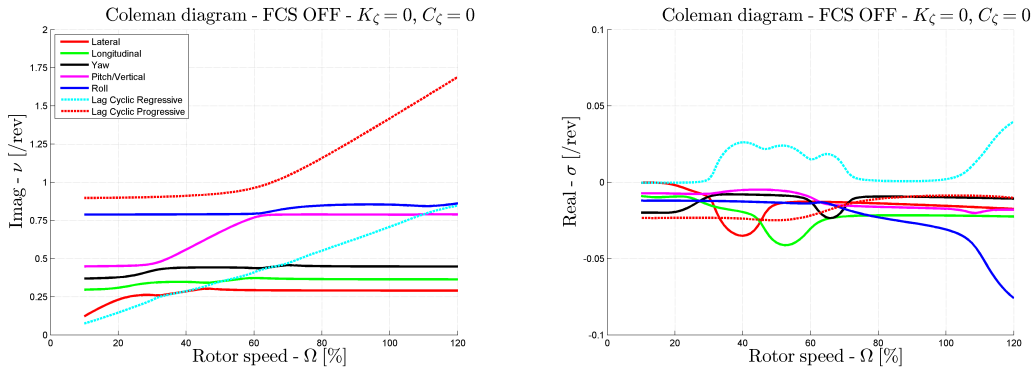

(a) (b)

Figure 2: Coleman diagrams for the evolution of the helicopter model eigenvalues with rpm; case with no lead-lag dampers, i.e. $K_\zeta = C_\zeta = 0$.

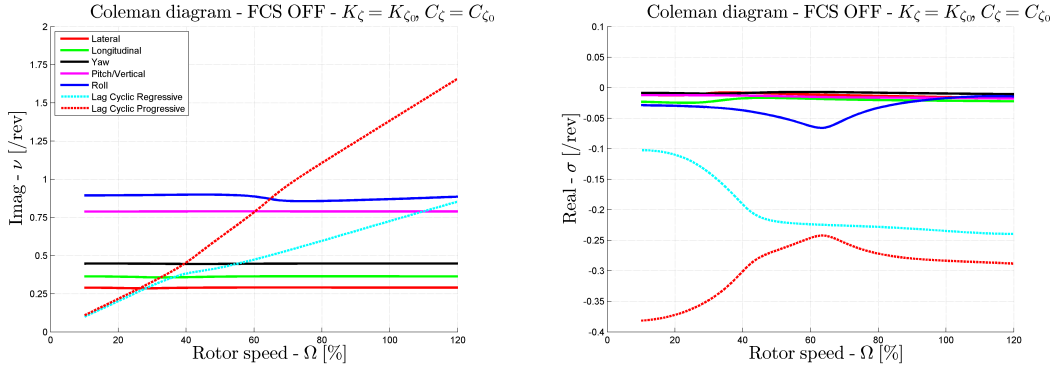

(a) (b)

Figure 3: Coleman diagrams for the evolution of the eigenvalues of the helicopter model with rpm; case with nominal lead-lag dampers, i.e. $K_\zeta = K_{\zeta_0}$, $C_\zeta = C_{\zeta_0}$.

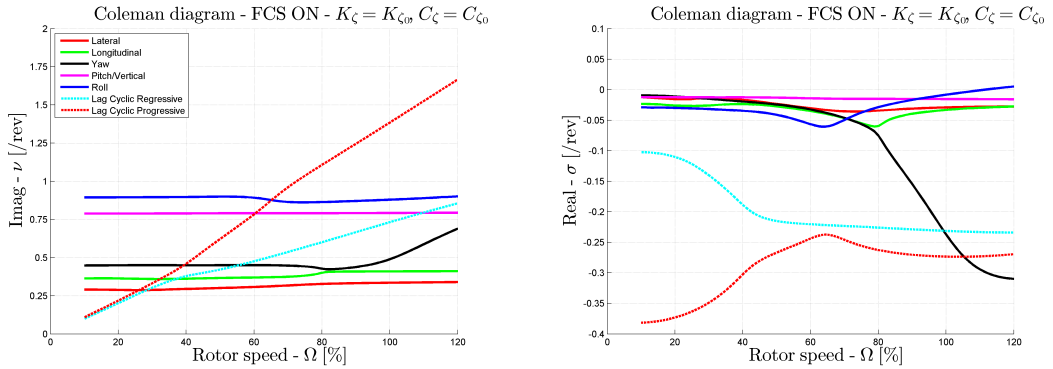

(a) (b)

Figure 4: Coleman diagrams for the evolution of the helicopter model eigenvalues with rpm; case with nominal lead-lag dampers and FCS.

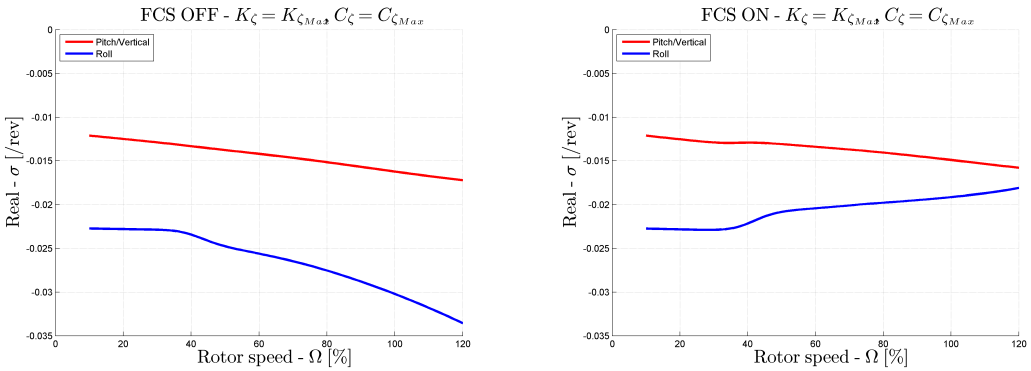

(a) FCS off

(b) FCS on

Figure 5: Evolution of the damping of roll mode with and without FCS.

SC effect.

In order to deepen the understanding of the instability generated by the introduction of the FCS, several additional analyses have been performed. Initially a basic GR model has been considered, excluding the FCS and the flapping modes. The rotor angular velocity is at 100% and $K_\zeta = 0$, while the lead-lag damping is the parameter that drives the analysis, and it goes from $C_\zeta = 0$ to the maximum value $C_{\zeta\,\text{max}}$. When lead-lag damping is null the lead-lag regressive mode is slightly unstable, as shown in Figure 6. By increasing the damping the mode becomes rapidly stable and remains stable. Adding damping about the lead-lag hinge the frequencies of the roll and pitch modes cross the regressive mode, and so the mode shapes are hybridized. By adding the flapping modes, the instability almost disappears at null damping. This analysis confirms that neglecting the flapping modes seems in general conservative from the stability point of view. However, it is possible to see how less damping is associated to the roll mode that becomes even lower when lead-lag hinge damping is added to the rotor. The inclusion of the FCS causes a shift of the real part of the roll eigenvalue toward zero, eventually becoming slightly unstable for high lead-lag damping values. This behavior reveals a potentially dangerous mechanism of initial reduction of roll damping with the increase of lead-lag hinge damping that may require a thorough analysis considering also the nonlinear behavior of the lead-lag dampers. These analyses would guarantee that no Limit Cycle Oscillation (LCO) conditions appears.

A summary of all these effects is obtained by looking at the stability maps shown in Figure 7. The bold black lines show the stability boundaries for different values of lead-lag stiffness and damping; the white zones are stable, while the colored zones are unstable; the color scale represent the maximum value of the positive damping of the eigenvalues. For the case with FCS off at 100% rpm a very small value of damping is sufficient to avoid any instability problem, while at 120% the unstable area is larger, although still confined close to the low values of lead-lag damping. For the cases with the FCS on the situation is different since also large damping values may cause instability, especially at 110% and 120% rpm.

5 Gain and Phase Margins

Although stability results are very important, a better picture can be obtained by analyzing the robustness of the FCS feedback loop with the helicopter. Using the definition given by Friedland [24], the degree of robustness can be defined as the level of immunity to uncertainty or changes of the plant. For Single Input Single Output (SISO) systems the classical approach suggests to compute the gain and phase margins. The gain margin is the minimum change in the loop gain, at nominal phase, which results in an instability, while the phase margin is the minimum change in phase, at nominal loop gain, which results in instability.

For Multiple Input Multiple Output (MIMO) systems, there have been defined several criteria that try to keep into account the intrinsic multi-loop structure of the problem [25, 26]. However, no single criterion is established as the standard for full assessment of closed-loop MIMO system robustness. Currently the SAE-AS94900 [27] suggests to compute the classical phase and gain margins of SISO systems opening one loop at a time, with

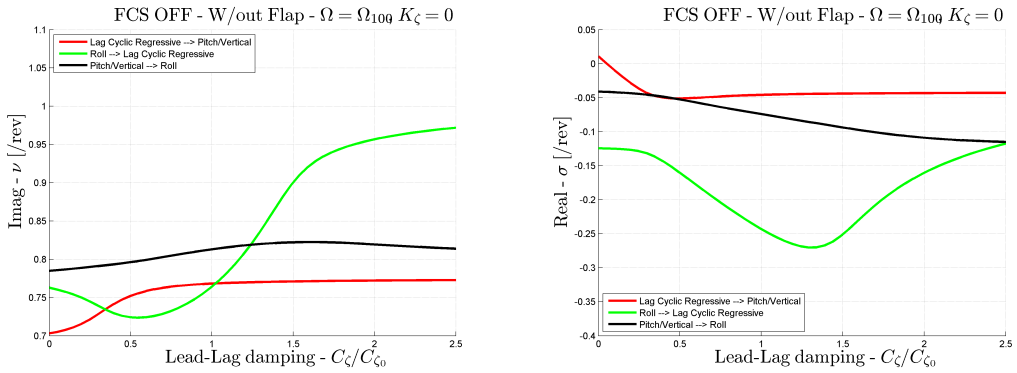

(a) Without flapping modes

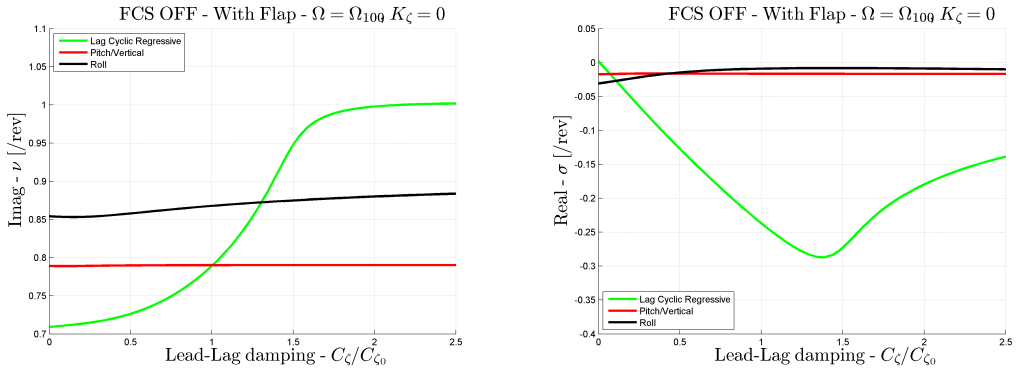

(b) With flapping modes

Figure 6: Evolution of the frequency and damping for different values of C_ζ, at 100% rpm, FCS off.

all the other feedback paths held at their nominal values, breaking the loops at the actuator commands. In this situation, with respect to aeroelastic modes, to be safe the SAE-AS94900 [27] suggests to ensure a gain margin of 8 dB and a phase margin of 60 deg.

Using MASST the gain and phase margins can be computed as functions of the rotating speed for nominal lead-lag damper characteristic values $K_{\zeta 0}$ and $C_{\zeta 0}$. Figure 8 shows the gain margins computed opening the loops at actuator commands. While the tail rotor actuator and the main rotor actuator #3 (the one not activated for a lateral cyclic) do not present any problem, the other two cross the safety margins. In particular actuator #2 of the main rotor crosses the margins at 97% rpm, indicating that this system, although formally stable, cannot be considered robust enough at the nominal speed. Close to 110% the margin goes to zero as expected because the system actually becomes unstable. The phase margin diagram of Figure 8 shows a slight border crossing of the tail rotor loop, but again the main problem is related to actuators #1 and #2 of the main rotor, which just after 100% rpm drop from an infinite phase margin to values below the level considered safe. To check if the particular choice of loops to be opened is influencing the results, an additional analysis has been performed opening the loops on sensors. In this case there are three loops that result in the diagrams shown in Figure 9. These analyses confirms that the gain margin falls below safety at around 90% rpm and that the instability is essentially related to the feedback loop on the roll axis.

6 Conclusions

The paper highlighted the importance of performing Structural Coupling analysis during the development of new rotorcraft designs that include a Flight Control System. It highlighted how the Flight Control System, designed to improve the handling qualities, may have an impact on the aeroelastic stability of the machine, and in particular on

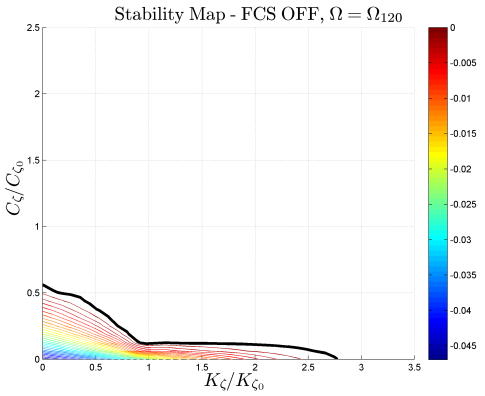

(a) 120% FCS off

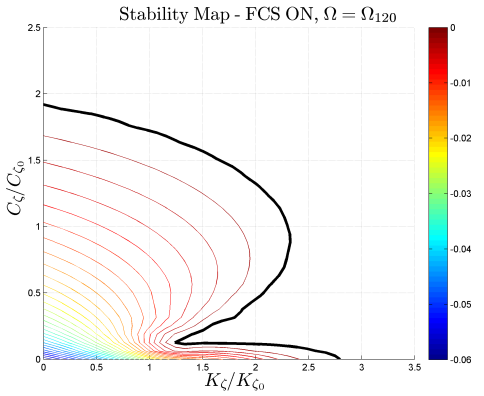

(b) 120% FCS on

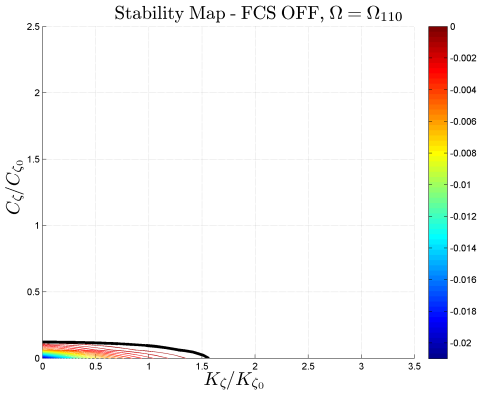

(c) 110% FCS off

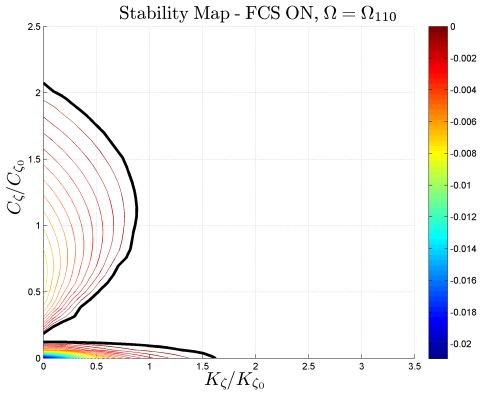

(d) 110% FCS on

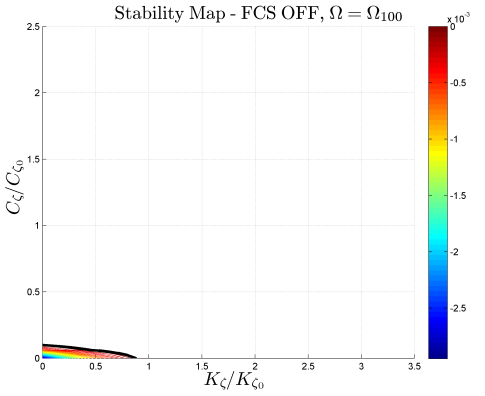

(e) 100% FCS off

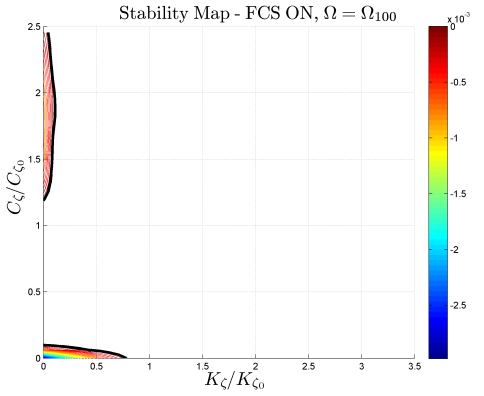

(f) 100% FCS on

Figure 7: Stability maps for different values of lead-lag damper characteristics K_ζ and C_ζ.

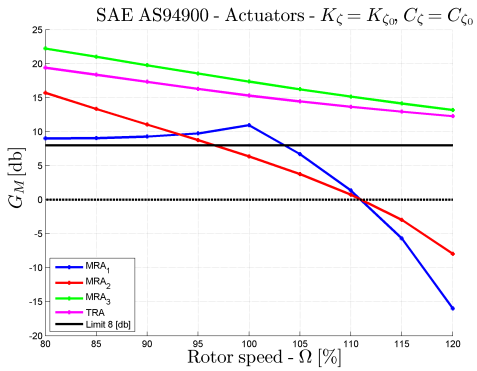

(a) Gain Margin

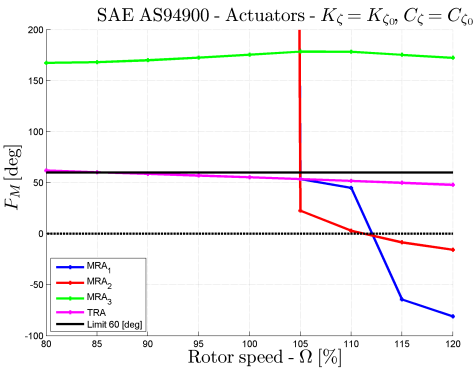

(b) Phase Margin

Figure 8: Evolution of gain and phase margins computed using the SAE-AS94900 approach with loops opened at the actuators.

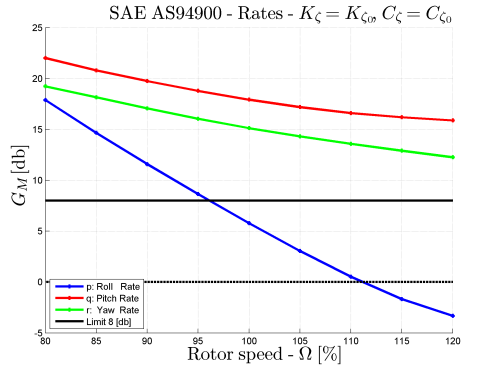

(a) Gain Margin

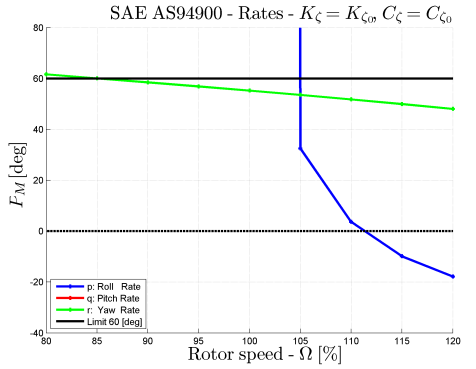

(b) Phase Margin

Figure 9: Evolution of gain and phase margins computed using the SAE-AS94900 approach with loops opened at the angular rate sensors.

the ground resonance phenomenon. The analysis of the gain and phase margins represents a valid tool to help engineers in identifying the robustness of the design. These preliminary analyses allow to identify modifications of the FCS to prevent it from interfering with aeroelasticity, while minimizing their impact on the overall performances. The effectiveness of MASST in performing this kind of analysis has been shown, since all the required elements can be modeled with an adequate level of detail.

REFERENCES

[1] L. R. Stiles, J. Mayo, A. L. Freisner, K. H. Landis, and B. D. Kothmann. "Impossible to resist" the development of rotorcraft fly-by-wire technology. In *AHS 60th Annual Forum*, Baltimore, MD, June 8-10 2004.

[2] J. Becker, B. Caldwell, and V. Vaccaro. The interaction of flight control system and aircraft structure. In *RTO AVT Specialists' Meeting on Structural Aspects of Flexible Aircraft Control*, Ottawa, Canada, 18–20 October 1999.

[3] Wayne Johnson. Development of a comprehensive analysis for rotorcraft — I. rotor model and wake analysis. *Vertica*, 5:99–129, 1981.

[4] Wayne Johnson. Technology drivers in the development of CAMRAD II. In *American Helicopter Society Aeromechanics Specialists Conference*, San Francisco, California, January 19–21 1994.

[5] G. Bir and Indeerit Chopra. *University of Maryland Advanced Rotor Code (UMARC) Theory Manual*. University of Maryland Center for Rotorcraft Education and Research, College Park, MD, November 1991.

[6] B. Benoit, A.-M. Dequin, K. Kampa, W. von Grünhagen, P. M. Basset, and B. Gimonet. HOST, a general helicopter simulation tool for Germany and France. In *56th Annual Forum of the American Helicopter Society*, Virginia Beach, May 2000.

[7] P. Masarati, D.J. Piatak, G. Quaranta, J.D. Singleton, and J. Shen. Soft-inplane tiltrotor aeromechanics investiga-

tion using two comprehensive multibody solvers. *Journal of the American Helicopter Society*, 53:179–192, 2008. doi:10.4050/JAHS.53.179.

[8] T. Parham, Jr. and Lawrence M. Corso. Aeroelastic and aeroservoelastic stability of the BA 609. In *25th European Rotorcraft Forum*, Rome, Italy, September 14–16 1999.

[9] P. Masarati, V. Muscarello, and G. Quaranta. Linearized aeroservoelastic analysis of rotary-wing aircraft. In *36th ERF*, Paris, France, September 7-9 2010.

[10] Robert P. Coleman and Arnold M. Feingold. Theory of self-excited mechanical oscillations of helicopter rotors with hinged blades. REPORT 1351, NACA, 1958.

[11] G. Reichert and U. Arnold. Active control of helicopter ground and air resonance. In *16th ERF*, Glasgow, Scotland, September 18–21 1990.

[12] G. Tettenborn, C. Kessler, and G. Reichert. Comparison of IBC with active controllers using a conventional swashplate to suppress ground and air resonance. In *23rd ERF*, pages 13.1–19, Dresden, Germany, September 16–18 1997.

[13] Roy R. Craig, Jr. and Mervyn C. C. Bampton. Coupling of substructures for dynamic analysis. *AIAA Journal*, 6(7):1313–1319, July 1968.

[14] Wayne Johnson. *Helicopter Theory*. Princeton University Press, Princeton, New Jersey, 1980.

[15] D. Levin. The approximation power of moving least-squares. *Mathematics of computation*, 67(224):1517–1532, 1998.

[16] Herbert E. Merritt. *Hydraulic Control Systems*. John Wiley & Sons, New York, 1967.

[17] M. Mattaboni, G. Quaranta, and P. Mantegazza. Active flutter suppression for a three-surface transport aircraft by recurrent neural networks. *Journal of Guidance, Control, and Dynamics*, 32(4), 2009.

[18] Wayne Johnson. *CAMRAD/JA, A Comprehensive Analytical Model of Rotorcraft Aerodynamics and Dynamics, Johnson Aeronautics Version*. Johnson Aeronautics, 1988.

[19] FK Straub. Optimal control of helicopter aeromechanical stability. *Vertica*, 11(3):425–435, 1987.

[20] M. Battipede, P.A. Gili, L. Carano, and V. Vaccaro. Constrained notch filter optimization for a fly-by-wire flight control system. *Aerotecnica Missili & Spazio*, 88(3):105–113, 2009.

[21] O. Dieterich, J. Götz, B. DangVu, H. Haverdings, P. Masarati, M. Pavel, M. Jump, and M. Gennaretti. Adverse rotorcraft-pilot coupling: Recent research activities in europe. In *34th European Rotorcraft Forum*, Liverpool, UK, September 16–19 2008.

[22] C.J. Bauer. A landing and takeoff control law for uniquetrim, fly-by-wire rotorcraft flight control systems. In *19th ERF*, Como, Italy, 1993.

[23] M. Pavel, J. Malecki, B. DangVu, P. Masarati, M. Genaretti, M. Jump, H. Smaili, A. Ionita, and L. Zaicek. Present and future trends in aircraft and rotorcraft pilot couplings — a retrospective survey of recent research activities within the european project ARISTOTEL. In *37th ERF*, Gallarate, VA, Italy, September 13–15 2011.

[24] B. Friedland. *Control System Design. An Introduction to State Space Methods*. McGraw Hill, New York, NY, 1987.

[25] S. Skogestad and I. Postlethwaite. *Multivariable feedback control – analysis and design*. Wiley, 2005.

[26] P. Masarati, V. Muscarello, and G. Quaranta. Robust aeroservoelastic stability of helicopters: application to the air/ground resonance. In *AHS 67th Annual Forum*, Virginia Beach, VA, May 3–5 2011.

[27] Anon. Aerospace - flight control systems - design, installation and test of piloted military aircraft, general specification for. AS 94900, SAE International, 2007.